12 September 1980, Volume 209, Number 4462 SCIENCE

High-Frequency Skywave Radar Measurements of Hurricane Anita

Joseph W. Maresca, Jr., and Christopher T. Carlson

Our purpose in this article is to describe the capability of remotely monitoring hurricanes and other open ocean storms by using a high-frequency (HF) skywave radar. We used this technique in 1977 to monitor, from California, hurricane Anita in the Gulf of Mexico. Using the SRI-operated Wide Aperture Research Facility (WARF) (*1*), we measured significant wave height, surface wind speed and direction, and surface current speeds for this first hurricane of the 1977 season. We recorded sea backscatter for the hurricane at distances of more than 3000 kilometers from the WARF by means of single F-layer ionospheric reflection. We compiled real-time maps of the surface wind direction field within a radial distance of 200 km of the storm center, then estimated the hurricane position from these radar wind maps and developed a track for Anita over a 4-day period between 30 August and 2 September 1977 as the storm moved westward across the Gulf of Mexico. The radar track was computed from 17 independent position estimates made before Anita crossed the Mexican coast, and was subsequently compared to the official track produced by the National Hurricane Center (NHC). Agreement between the WARF position estimates and coincident temporal positions on the NHC smooth track was ± 19 km.

Summary. We tracked and monitored hurricane Anita over a 5-day period by using the SRI-operated Wide Aperture Research Facility (WARF) high-frequency skywave radar. The WARF-derived positions for Anita agreed to within ± 19 kilometers of the coincident temporal positions along the National Hurricane Center's smooth track. Hurricane Anita passed near the open ocean-moored buoy EB-71 of the National Oceanic and Atmospheric Administration, and measurements of wind direction, wind speed, and significant wave height made during this period at the WARF and in situ at the buoy showed agreement of 7°, 0.4 meter per second, and 0.5 meter, respectively. The WARF estimates of longshore coastal surface currents showed good agreement with measurements made at a moored current meter.

At approximately 0000 G.M.T. on 1 September 1977, Anita passed within 50 km of the open ocean-moored buoy EB-70 (26.0°N, 93.5°W) of the National Data Buoy Office (NDBO) of the National Oceanic and Atmospheric Administration (NOAA) and enabled us to compare WARF estimates of the significant wave height and surface wind speed and direction in all four quadrants of the storm with those made at the buoy. Agreement between the WARF and EB-71 measurements was within 10 percent. We measured the surface currents along the western Louisiana coastline by using the WARF radar, and our measurements show good agreement with those made by moored current meters. In addition to describing the important aspects of the WARF skywave radar, we discuss here the sea-echo Doppler spectra, the method of analysis used to estimate the wind-wave and surface current parameters, and the accuracy of these radar-derived quantities (*2*, *3*).

J. W. Maresca, Jr., is a senior oceanographer and C. T. Carlson is an oceanographer with the Remote Measurements Laboratory of SRI International, Menlo Park, California 94025.

WARF Skywave Radar

The WARF is a high-resolution, experimental, HF skywave radar located in central California. The radar is bistatic and operates in the HF band between 6 and 30 megahertz. Ocean areas are illuminated by a 20-kilowatt swept-frequency continuous-wave signal from a transmitter site located at Lost Hills, California. The energy reflected from the surface beam is received 185 km to the north at Los Banos, California. The receiving antenna array is 2.5 km long and consists of a double linear array of 256 whip antennas producing a nominal 1/2° azimuthal beamwidth at 15 MHz. The signal propagates to and from remote ocean patches by means of one or more ionospheric "reflections."

The WARF coverage area is shown in Fig. 1. The radar can be directed either east or west, and can be electronically steered in azimuth ± 32° from boresight anywhere within the coverage area in 1/4° increments. Position accuracy is a function of midpath ionospheric height estimates whose uncertainty results in a nominal position accuracy of approximately 20 km. However, at any one location the accuracy between consecutive measurements in range and azimuth is an order of magnitude better. WARF has multiple-beam capability, and sea backscatter is usually received simultaneously at four adjacent ocean areas from four different beams separated by 1/4°. The size of the ocean scattering patch is a function of the beamwidth, the range, the range cell separation, and the number of range cells averaged together. The size of the minimum scattering patch at a range of approximately 2000 km is 3 km in range by 15 km in azimuth.

0036-8075/80/0912-1189$02.00/0

Sea-Echo Doppler Spectrum

The sea backscatter received at the WARF is coherently processed in range and Doppler shift to produce a sea-echo Doppler spectrum. We usually process 21 independent Doppler spectra spaced at 3-km intervals. These spectra are obtained simultaneously at each of four adjacent radar beams. A total of 84 independent Doppler spectra are obtained for each coherent time period. We compute an average spectrum from a subset of these Doppler spectra, depending on the type of measurement and the time and space scales associated with the ocean surface features. An example of a mean sea-echo Doppler spectrum which was produced by averaging 112 spectra obtained from four consecutive 102.4-second coherent time periods, over a scattering patch consisting of 21 range cells and three adjacent beams, is shown in Fig. 2.

The sea-echo Doppler spectrum (see Fig. 2) is characterized by two dominant first-order echoes surrounded by a second-order continuum. Crombie (*4*) interpreted the first-order echoes in terms of simple Bragg scattering that represented a resonant response between radio waves of wave number k_0 and ocean waves of wave number $k = 2k_0$. The radar measures the relative power and Doppler shift of the ocean waves traveling radially toward or away from the radar. The power ratio of the two first-order echoes is indicative of the direction of the waves of wave number k. Because k is usually large ($k > 0.5$), it is assumed that the wind direction is identical to the direction of these waves. Any shift in Doppler frequency of the first-order echoes from their theoretical positions when the ionospheric Doppler shift is zero is indicative of the magnitude of the surface current.

The wave height spectrum is derived from the second-order structure surrounding the first-order echoes. For hurricanes, the power in the second-order echoes increases as illustrated in Fig. 3. Barrick (*5, 6*) derived theoretical expressions that accurately model the HF scattering process to second order. For a specific directional wave spectrum, the model computes the Doppler spectrum. The effects of the wind direction, wave directionality, and wave frequency spectrum on the modeled Doppler spectrum have been extensively studied through the use of this model.

Hurricane Data Sampling

Data sampling during a hurricane is divided into two tasks to optimize the sampling time and the data quality. The spectral resolution, directly related to the coherent integration time, can be much coarser for first-order measurements than for second-order measurements. Wind direction estimates are computed from the first-order echoes, and can be computed considerably more rapidly than wave height and wind speed estimates, which are computed from the second-order echoes. Usually, the longer the coherent integration time, the greater the influence the ionosphere has on the quality of the data.

The quality of the recorded sea backscatter depends on the ionospheric conditions over short periods—on the order of minutes. High-quality sea backscatter is obtained if the radio waves propagate by means of a strong, single, stable, coherent ionospheric layer. Sometimes the signals may be received at the same time from two or more different paths (multipath). In this case, the second or succeeding signals will be reflected from different parts of the ocean and different parts of the ionosphere, and will contaminate the sea echo received from the first path.

If the ionosphere is changing in time or space during the coherent radar dwell (time period), further degradation of the data will occur. The ability to predict the ionospheric conditions would enable the radar operator to minimize the contaminating effects of the ionosphere, improve the quality of sea backscatter, and reduce the sampling time. The ionospheric soundings provide some information on the quality of the data obtained. The vertical and oblique incidence soundings are taken every 10 minutes; a complete sounding requires approximately 3 minutes. The coherent radar measurements made at WARF require between 10 and 100 seconds to complete. Because the time required to complete a sounding is greater than the time required to record the sea backscatter data, assessment of the data quality is difficult for rapidly changing ionospheres. Therefore, real-time output of the data from the WARF site minicomputer is used to verify data quality.

The wind direction measurement is not extremely sensitive to ionospheric contamination because only the amplitude of the two strong first-order echoes must be measured. A coherent integration time of 12.8 seconds (0.078 Hz resolution) is sufficient to resolve the peaks of the first-order echoes. We can map the surface wind direction field of a hurricane in about 10 minutes. Once the surface wind direction map is made, the storm center can be identified for tracking purposes, and regions of interest can be selected for more extensive monitoring of wind speed and wave height anywhere within the storm.

The measurement of surface currents by HF radar is slightly more sensitive to contamination of the Doppler spectrum by ionospheric multipath or smearing than the wind direction measurements. The surface current measurements are based on the Doppler shift of the first-order echoes relative to an echo of known Doppler shift. To resolve accurately the Doppler shifts of these echoes, coherent integration times of 102.4 seconds (0.01 Hz resolution) are used to process the data. The accuracy of the surface current estimate is a function of the ability to identify clearly the peak of the first-order echoes.

The significant wave height and wind speed measurements are sensitive to ion-

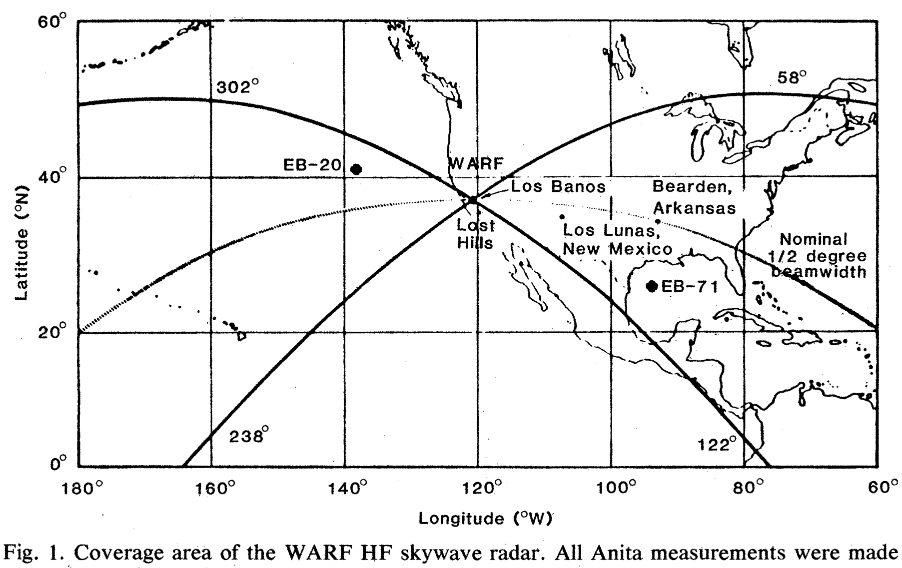

Fig. 1. Coverage area of the WARF HF skywave radar. All Anita measurements were made west of 88°W in the Gulf of Mexico.

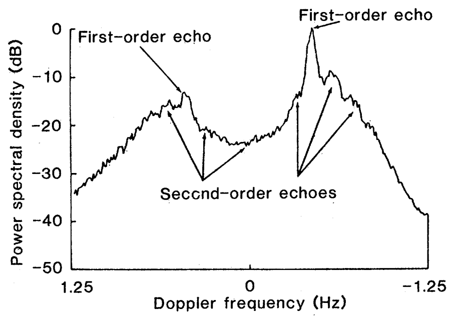

Fig. 2. Average sea-echo Doppler spectrum recorded within 35 km of the center of hurricane Anita at 2343 G.M.T. on 31 August 1977.

ospheric contamination because these quantities are estimated from the second-order echoes surrounding the stronger first-order echoes. This contamination is the largest source of error in these measurements. A coherent integration time of 102.4 seconds is required to resolve the second-order echoes. The ionosphere does not generally support coherent integration time periods of this length. Multipath and ionospheric smearing can seriously degrade the weaker second-order echoes. This contamination would prevent us from routinely estimating wave height for each 102.4-second time period, although we are able to calculate the surface current for each 102.4-second period or wind direction for each 12.8-second time period. In order to obtain a data set suitable for analysis, we use a sampling strategy that combines careful propagation management that results in a stable, coherent, single propagation path, and signal processing that minimizes the contaminating effects of the ionosphere. Recent work by SRI and NOAA (*7*) has resulted in improved methods of collecting high-quality data by sorting the data according to a spectral sharpness index. The effect of ionospheric contamination, however, is less severe for data recorded during large ocean wave conditions generated during a hurricane. The amplitude of the second-order echoes containing the wave height information may be stronger than the contamination effects, and wave height can therefore be calculated despite the contamination.

For the wind direction measurements on Anita, we divided the data into 16 groups and analyzed three consecutive 12.8-second coherent radar dwells. Each wind direction estimate was calculated from a minimum of 15 Doppler spectra. At a range of 3000 km, the size of each scattering patch was 15 by 25 km. It would be desirable to compute wave height and wind speed from a similar data set, but this is not generally possible. Longer, coherent integration periods and more independent samples of the spectra are required to obtain a high-quality sample. We could collect the data over a small scattering patch by averaging over a long time, or we could increase the scattering patch size and average in space. Averaging in space is preferable because it reduces the total time required to obtain a mean Doppler spectrum. For the wave height and wind speed measurements on Anita, we analyzed the data from three of the adjacent azimuth cells and 21 contiguous range cells. The total scattering patch was 50 by 63 km. Several consecutive integration periods are required to record the data.

Wind Direction

High-frequency skywave radar has been used to map the surface wind fields associated with large weather systems (*8*) and tropical storms (*9*). The radar-measured surface wind directions are derived from the predominant direction of ocean gravity waves, approximately 10 meters long. The waves satisfying the first-order Bragg scattering condition, $k = 2k_0$, are assumed to be tightly coupled to the wind for time scales on the order of tens of minutes. This assumption is reasonable for the high wind speed conditions associated with hurricanes. Available measurements of directional wave spectra (*10–12*) indicate that the dominant wave direction is representative of the predominant wind direction. For open ocean conditions, agreement between the WARF radar and shipboard anemometer measurements of wind direction is ± 16° (*13*). For hurricane winds, the agreement between coincident wind direction measurements made by NDBO data buoys and the WARF radar is better than 10° (*2, 3, 9*).

The radar measures the relative power between the approaching and receding waves that satisfy the Bragg scattering condition. If a cosine directional distribution $[G(\theta)]$ (*10*),

$$G(\theta) = \cos^s(\theta/2) \qquad (1)$$

is assumed, then the relative power of the approaching and receding waves measured by the radar is sufficient to estimate θ with an ambiguity about the beam direction. This left-right ambiguity is resolved by the predictable cyclonic surface circulation within the hurricane. The shape of $G(\theta)$ is controlled by the ocean conditions; we have estimated s from several models (*12, 13*). For the maximum hurricane winds, the values of s estimated from these models are too low. On the basis of previous hurricane analyses and spot measurements of wind direction at NDBO data buoys, we used values of s of 1.0 or 2.0. No attempts were made to account for variations in s as a function of location within the hurricane.

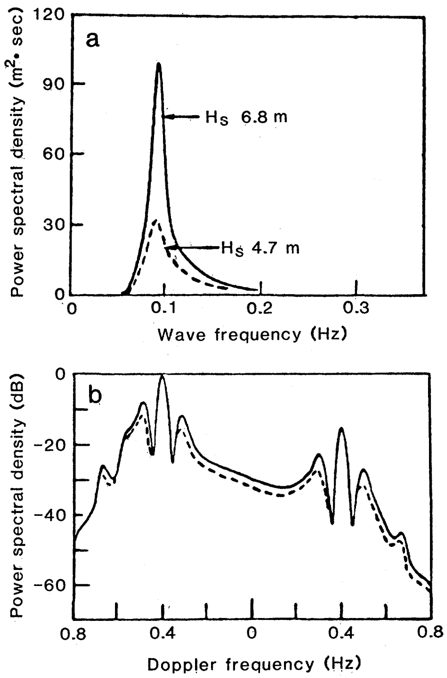

Fig. 3. Example of two synthetic Doppler spectra (b) produced from two input wave spectra (a) with the same directional distribution and radar-to-wind direction, but different total wave energy (0.02 Hz resolution).

Surface Current

The speed of the surface currents directed radially to the radar in the upper 1 m of ocean may be estimated from the phase speed, or Doppler shift, of the ocean waves producing the first-order sea echoes (*14–17*). The measured phase velocity of these ocean waves may be different from the theoretical phase velocity predicted by first-order water-wave theory. This difference is caused by the advection of the waves by a current. Stewart and Joy (*16*) showed that the surface current $V(Z)$ at depth $Z = d$ is

$$V\left(d = \frac{L}{4\pi}\right) = L\,\Delta\omega \qquad (2)$$

where L is the ocean wave length, and $\Delta\omega$ is the shift in Doppler frequency of the first-order echoes. For a radar frequency of 15 MHz and a Doppler shift of 0.05 Hz, the magnitude of the surface current directed radially along the radar axis is 0.50 m/sec at a depth of 0.80 m. Unlike the surface wave HF radar wind direction measurement, the effects of the ionospheric motion must be known to make a skywave measurement of current. The entire Doppler spectrum can be shifted by ionospheric motion. It has been shown (*2, 18, 19*) that echoes received from an HF repeater, from land, or from oil platforms during coastal scans along the Gulf of Mexico are sufficient to remove the effects of the ionospheric motion from the data. After removal of the ionospheric effects from the Doppler spectrum, we assume that any deviation from the theoretically predicted Doppler shift of the first-order peaks is due to the surface current.

The radar-measured component of the surface current is directed along the radar axis. With only one radar measurement, the absolute component of the current cannot be derived. A second independent measurement by a radar with overlapping coverage would be required for an absolute direction measurement. However, the radar axis is approximately parallel with the Gulf of Mexico coastline in the region of measurement reported here and provides a reasonable estimate of longshore surface-current velocity.

Significant Wave Height

Barrick (*5, 6*) derived an integral expression that predicts the Doppler spectrum for a specific directional wave spectrum input. Recent efforts have succeeded in inverting this integral expression to compute the input root-mean-square (r.m.s.) wave height (*20, 21*), one-dimensional wave frequency spectrum (*22–27*), and the directional distribution (*23–27*). The expressions of Barrick (*20, 22*) have been used to analyze skywave radar data recorded for a Pacific Ocean storm (*21*) and tropical storms (*2, 3, 28*).

We used a power law derived from simulated data by Maresca and Georges (*21*) to compute r.m.s. wave height by relating the ratio of the total second-order and first-order power to the r.m.s. wave height:

$$k_0 h = aR^b \quad (3)$$

where $0.2 < k_0 h < 1.0$, h is the r.m.s. wave height; k_0 is the radar wave number; R is the ratio of the total second- to total first-order power; and $a = 0.8$ and $b = 0.6$ are constants. This average expression was derived from theoretical simulations of the Doppler spectra for different radar to wind directions, directional distributions, functional forms of the wave frequency spectrum, and operating radar frequencies. Equation 3 is accurate to within 15 percent. The errors have been discussed (*2, 3, 21*).

Wind Speed

Historically, wave models have been developed to predict wave height and the wave spectrum from an input wind field. The accuracy of these models depends on the accuracy of the input winds. Hasselmann *et al.* (*29*) proposed a one-dimensional parametric wind-wave model for fetch-limited growing wind-sea conditions. Ross and Cardone and co-workers (*30–33*) empirically derived a power-law expression for hurricanes based on the form proposed by Hasselmann *et al.* (*29*) that relates the nondimensional wave energy, $\tilde{E}$, by using wind, wave, and fetch measured during hurricanes Ava, Camille, and Eloise. For hurricanes,

$$\tilde{E} = 2.5 \times 10^{-5} \tilde{R}^{0.45} \quad (4)$$

where $\tilde{E} = Eg^2/W^4$; $\tilde{R} = rg/W^2$; $E = h^2$; and $H_s = 4h$. In $\tilde{E}$ and $\tilde{R}$, E is the total wave energy, h is the r.m.s. wave height; H_s is the significant wave height; r is the radial distance from the eye to the measurement point that accounts for fetch; g is the gravitational acceleration; and W is the wind speed. Solving for wind speed in Eq. 4, we obtain

$$W = \left(\frac{h^2 g^2}{2.5 \times 10^{-5}\,(rg)^{0.45}}\right)^{0.323} \quad (5)$$

The wind-wave model used to derive Eq. 5 is applicable for slow-moving storms in which $W \geq 15$ m/sec, and $\tilde{R} \lesssim 3 \times 10^4$. For the unusual cases where the storms move very fast or very slow, Ross and Cardone (*32*) showed that significant differences occur in the modeled and measured wave height.

We used Eq. 5 to calculate wind speed for Anita and compared our results with the 15-minute wind speed estimates made at NDBO buoys and by reconnaissance aircraft. The radial fetch (r) was measured from the WARF-derived wind maps, and the wave height (h) was computed using Eq. 3. The radar-derived W is not an instantaneous wind speed estimate; it is a temporal and spatial average of the winds.

Measurements and Results

Hurricane Anita formed as a tropical depression in the Gulf of Mexico at about 1200 G.M.T. on 29 August 1977. Anita developed into a tropical storm at approximately 0600 G.M.T. on 30 August 1977, and about 12 hours later intensified into the first Gulf of Mexico hurricane of the 1977 season. As Anita moved west across the Gulf, winds in excess of 75 m/sec were recorded. Five days of skywave data, beginning 29 August 1977, were recorded prior to Anita's landfall, 2 September 1977, approximately 250 km south of Brownsville, Texas. Twenty-one radar wind maps were compiled at WARF. The first four wind maps were not used in the radar-derived track presented here because the radar showed two distinct centers during this early period.

On 30 August 1977, the storm intensified and developed one center. The wind maps were updated three to five times per day during both daytime and nighttime periods and were used to develop the WARF-derived track. Figure 4 shows the radar-derived positions in relation to the official NHC smooth track produced from reconnaissance aircraft measurements, visible and infrared satellite cloud photographs, and shore-based microwave radar. The relative agreement between the WARF position estimates and the interpolated temporal position estimates along the smooth track is ± 19 km (*34*).

There are two potential sources of error associated with the WARF hurricane position fixes: the absolute position error of the radar consisting of range and azimuth errors, and the errors associated with locating the storm center from the radar wind direction measurements. We estimate the range errors of the radar caused by errors in determining the ionospheric height at midpath to be 20 km. If a coastal scan is included as part of collecting the wind map data, the land echo can be used as a reference to more accurately determine the ionospheric height, and therefore reduce this error. We estimate the error in azimuth caused by ionospheric tilting to be 20 km. These range and azimuth errors can be reduced significantly by installing an HF repeater along the coast that receives signals and transmits them back with a known frequency shift. When we assume similar mean ionospheric conditions within 200 km of the storm center, the entire wind map can be translated in azimuth and range to correct for the absolute position error. The location of the wind direction measurement with respect to the storm center is generally not affected by these position errors. The error associated with determining the storm center from the radar maps is about 20 km. The error is caused by the left-right ambiguity in the wind direction measurement. The average maximum error from these two potential sources of error is about 40 km. In comparing the WARF position fixes to the NHC track we found relative differences of between 5 and 50 km, and these relative differences can be attrib-

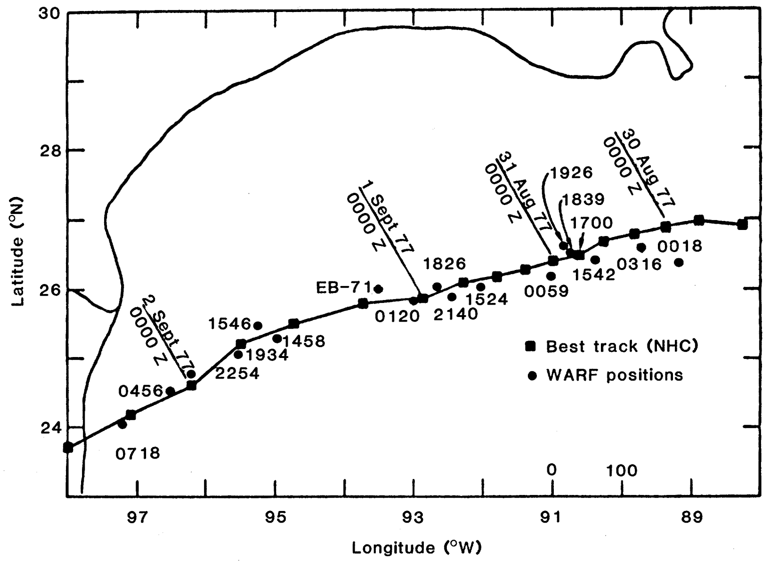

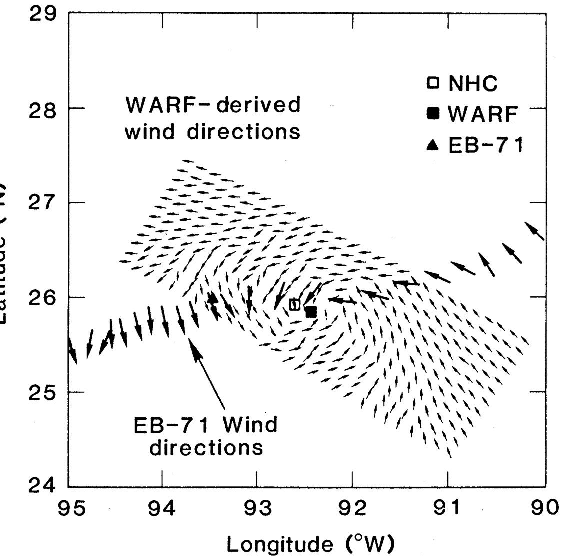

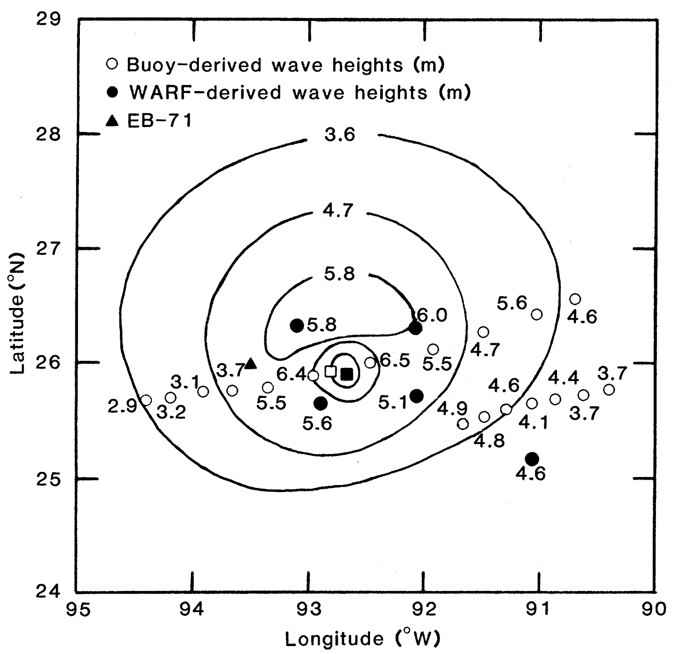

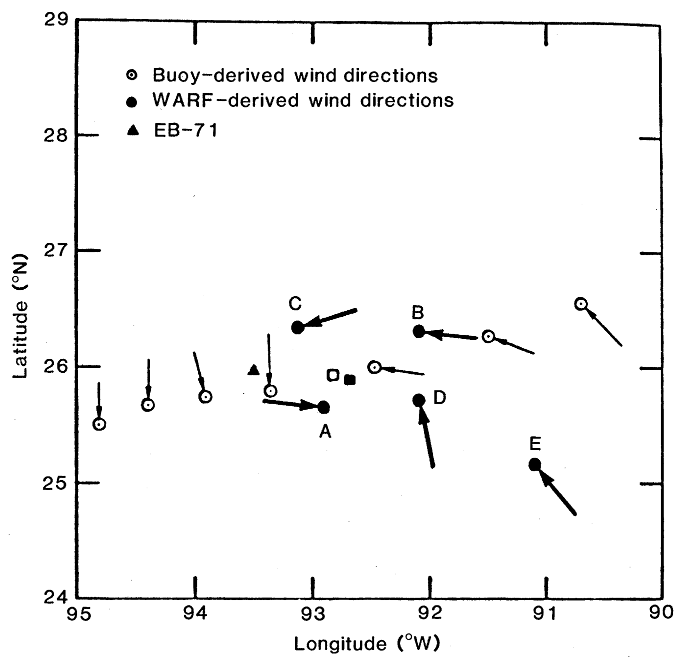

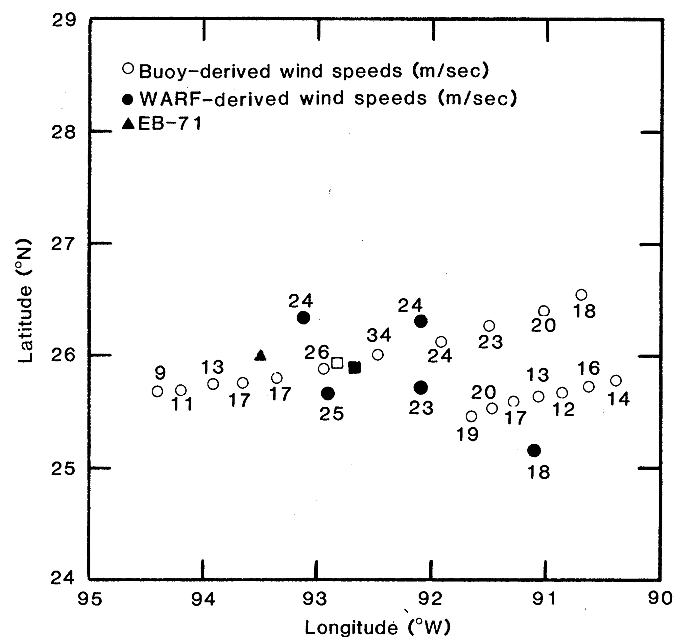

(Top row) Fig. 4 (left). WARF-measured track of hurricane Anita produced from the radar wind maps (Z = G.M.T.). Fig. 5 (right). WARF-derived wind direction map made for Anita at 2140 G.M.T. on 31 August 1977. (Middle row) Fig. 6 (left). Comparison of the WARF-derived significant wave heights measured between 2314 G.M.T. on 31 August 1977 and 0020 G.M.T. on 1 September 1977, and EB-04 and EB-71 derived significant wave heights measured between 0600 G.M.T. on 31 August 1977 and 1800 G.M.T. on 1 September 1977. The wave height contours are reproduced from figure 9 of Cardone *et al.* (*33*). The letter designations are given on Fig. 7. Fig. 7 (right). Comparison of the WARF-derived wind direction (→) made between 2314 G.M.T. on 31 August 1977 and 0020 G.M.T. on 1 September 1977 and the EB-71 derived wind directions (→) made between 0600 G.M.T. on 31 August 1977 and 1800 G.M.T. on 1 September 1977. (Bottom row) Fig. 8. Comparison of the WARF-derived wind speed measured between 2314 G.M.T. on 31 August 1977 and 0020 G.M.T. on 1 September 1977, and the EB-71 derived wind speed measured between 0600 G.M.T. on 31 August 1977 and 1800 G.M.T. on 1 September 1977.

uted to the sources of error just discussed.

Anita passed 50 km south of NDBO buoy EB-71 at about 0000 G.M.T. on 1 September 1977. Two WARF-derived wind maps were made at 2140 G.M.T. on 30 August 1977 and 0120 G.M.T. on 1 September 1977, which brackets this time period. One of these wind maps is shown in Fig. 5. Also shown in Fig. 5 is the surface wind direction field derived from data recorded by NDBO buoy EB-71. These buoy-measured wind directions were recorded at 2-hour intervals during the period ± 18 hours of Anita's passing EB-71. The buoy-derived wind field was computed by a time-space conversion that assumed uniform wind direction and lateral storm motion during this period. We compared the buoy-derived wind directions to the WARF-derived wind directions; agreement was within 16° ± 13°. Agreement between the WARF-derived wind direction estimate coincident in time and space with the buoy wind direction estimate was 1°.

Between 2314 G.M.T. on 31 August 1977 and 0020 G.M.T. on 1 September 1977, WARF measurements were made at five locations surrounding the center of the storm. The location of each measurement relative to the storm center was interpolated from the two wind maps. We computed the wind direction by using Eq. 1, wind speed by using Eq. 5, and wave height by using Eq. 3 at each location (see Table 1), and compared these measurements to a buoy-derived wind and wave field. The maps of the

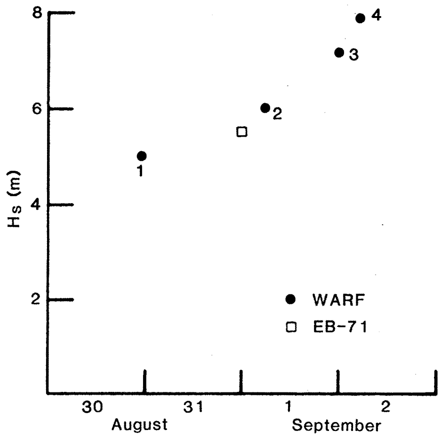

Fig. 9. Daily estimates of significant wave height for hurricane Anita made at the WARF radar.

spatial distribution of the wind direction, wind speed, and wave height were compiled from NDBO EB-71 and EB-04 data buoy measurements. Each parameter was plotted in relation to the storm center; they are shown in Figs. 6, 7, and 8. We assumed that Anita moved uniformly with no change in the meteorological conditions during the period 18 hours before and 18 hours after passing the buoy.

The significant wave height shown in Fig. 6 was measured at the buoy every 3 hours; the wind direction and wind speed shown in Figs. 7 and 8 were measured at the buoys every 6 hours and 3 hours, respectively. During this time period, Anita began to intensify, and under our assumption of uniform lateral storm motion the validity of the buoy-derived wind and wave fields are generally suspect. Exact comparisons of the EB-04, EB-71, and WARF measurements are difficult because of the differences in the time, location, and area of ocean monitored. In Fig. 6 we also included a wave hindcast for significant wave height based on the forecast computed by Cardone *et al.* (*33*) and our previous calculation (*35, 36*). We computed the significant wave heights from Eq. 4 using maximum sustained wind speed estimates made from central pressure, radius of maximum winds, and the true storm track. Equation 3-35 in (*37*) was used to estimate this maximum sustained wind speed for a storm moving at approximately 3 m/sec. The outer significant wave height contours were based on the same ratio of wave height to the maximum presented in (*35, 36*).

The WARF wind and wave height estimates were in general too far away from the buoy-derived quantities for direct comparison, but the agreement between the WARF- and buoy-derived wind and wave fields was reasonable. The buoy- and WARF-derived estimates of wave height were compared to the hindcast wave height estimates. WARF estimates of wave height at points A, B, C, and D, located at the extremes of the hindcast regions of highest waves, generally show good agreement with the hindcast. The WARF- and buoy-derived wave height measurements show reasonable spatial continuity and suggest that possibly the 3.6- and 4.7-m hindcast contours should be shifted eastward. We should note that any contamination of the sea-echo Doppler spectra by the ionosphere would result in radar wave height estimates that would be too high. The composite of wave height data obtained from the hindcast, EB-04, and EB-71 buoys indicates the validity of the WARF wave height estimates.

The agreement between the WARF- and buoy-derived estimates of wind speed is reasonable. There are three principal errors associated with the WARF wind speed estimate: error in estimating the radial fetch, error in estimating the r.m.s. wave height, and error in the parametric model. We computed the error in calculating wind speed for a ± 0.5 m error in estimating wave height for significant wave height of 5.5 m (9.1 percent error) and for radial fetches of 30, 50, 70, and 100 km. The errors were less than 1.6 m/sec. We also computed the error in calculating wind speed for a ± 20 km error in estimating the radial fetch for a significant wave height of 5.5 m and radial fetches of 30, 50, 70, and 100 km. For radial fetches greater than

Table 1. WARF estimates of significant wave height (H_s), wind speed (W), and wind direction (ϕ). N, number of spectra averaged; r, radial distance.

Point	Latitude (°N)	Longitude (°W)	Time (G.M.T.)	r (km)	N	H_s (m)	W (m/sec)	ϕ (°N)
A	25.7	92.9	2314	35	80	5.8	26.7	277.5
A	25.7	92.9	2343	35	112	5.2	22.8	—
B	26.3	92.1	2324	75	80	6.0	24.4	95.1
C	26.3	93.1	2358	65	35	5.8	24.4	70.2
D	25.7	92.1	0003	65	134	5.1	22.5	168.8
E	25.2	91.1	0020	180	49	4.6	18.1	137.2

Table 2. Comparison of wind speed values calculated from Eq. 5 derived from EB-71 significant wave height measurements. H_s, wave height; r, radial distance.

Latitude (°N)	Longitude (°W)	H_s (m)	r (km)	Wind speed (m/sec)		Difference (m/sec)
				Computed	Measured	
25.5	94.8	2.5	217	11.9	7.6	+ 4.3
25.7	94.4	2.9	174	13.5	9.0	+ 4.5
25.7	93.9	3.1	124	14.9	13.3	+ 1.6
25.8	93.4	5.5	69	23.4	17.4	+ 6.0
26.0	92.5	6.5	24	30.4	34.1	− 3.7
26.3	91.5	4.7	126	19.4	23.1	− 3.7
26.6	90.7	4.6	212	17.7	18.1	− 0.4

30 km, a +, 20 km error causes an error of less than 2 m/sec in wind speed. For radial fetches greater than 50 km, a −20 km error causes an error of less than 2 m/sec in wind speed. This represents less than an 8 percent error. These errors are typical of the WARF estimates of the significant wave height and radial fetch measurements. The errors associated with the model are discussed by Ross and Cardone (*32*). For Anita, the mean and r.m.s. difference between the parametric model forecast (*33*) and measured wave heights at EB-71 is 0.21 ± 0.83 m. This includes errors in measuring wave height at the buoy and in radial fetch from the conventional position fixes.

We also calculated the wind speed using Eq. 5 for some of the buoy-measured wave heights shown in Fig. 6, and compared the calculated wind speed measurements to wind speeds measured at the buoy (Table 2). The data are indicative of the accuracy we could expect from the WARF estimates of wind speed using Eq. 5. For these data, we believe the largest sources of error in the comparison were the uncertainty in the radial distance to each point caused by compiling the map from data collected over a 36-hour period, and the assumption of a symmetrical distribution of the winds.

We computed wave height and wind speed estimates several times daily over the life of Anita. Figure 9 and Table 3 show daily wave height and wind speed estimates, respectively, made at several locations within the storm from 30 August through 2 September. Anita intensified over this period as reflected in the increasing wave heights. Also shown in Fig. 9 is the wave height measured in situ by EB-71 at 0000 G.M.T. on 1 September. Using Eq. 5 we estimated wind speeds from the WARF radar measurements of wave height and radial fetch. No other surface observations of wind speed were available for comparison to the radar data. However, estimates of wind speed obtained by NOAA reconnaissance aircraft at an altitude of 440 m and averaged over 5 seconds were available for this time period (*38*). Direct comparison of the aircraft wind speeds and the WARF radar wind speeds is difficult because of different altitudes, averaging times, and locations of the measurements. We reduced the aircraft flight-level wind speed to a surface-level wind speed for comparison to the WARF radar estimates. The aircraft measurements were made along N-S and E-W axes directed through the storm center. The aircraft measurements nearest the WARF radar measurements were used to estimate the surface wind speed. We computed the surface wind speed from the aircraft measurements using a ratio relating the upper-level gradient wind to the surface-level wind. Using the two-layer Cardone (*39*) marine boundary layer model, Elsberry *et al.* (*40*) computed the ratio of the wind at the top of the upper layer to the wind at the top of the surface layer for different regions of the hurricane, different surface roughness, and different ratios of heat conductivity to eddy viscosity. This ratio ranges from about 0.5 to 0.85. The lower values represent regions near the peak winds. We assumed that the 440-m aircraft wind was representative of the wind at the top of the upper layer and reduced it to the surface level using a ratio of 0.7.

The agreement between the WARF radar and aircraft winds corrected to the surface is good. This comparison is not intended as a test of the radar technique. The purpose of this comparison was to demonstrate that the WARF radar estimates of wind speed are quite reasonable and are considerably different from the upper level wind speed estimates.

Surface current measurements were made at the WARF radar during the periods 30 August through 2 September 1977 and 4 to 5 September 1977 (*41*). The measurements were made along the western portion of the Louisiana coastline as shown by the shaded region in Fig. 10a. Two days after Anita crossed the coastline, tropical storm Babe—a weaker,

Table 3. Comparison of wind speeds computed from Eq. 5 and measured by NOAA reconnaissance aircraft.

Point	Latitude (°N)	Longitude (°W)	WARF radar: Date (1977)	WARF radar: Time (G.M.T.)	WARF radar: r* (km)	WARF radar: H_s (m)	WARF radar: Surface W (m/sec)	NOAA aircraft: Date (1977)	NOAA aircraft: Time (G.M.T.)	NOAA aircraft: Wind speed (m/sec) At 440 m	NOAA aircraft: Wind speed (m/sec) At surface
1	27.7	92.3	30 August	2052	188	5.0	19.0	30 August	1326	23.0	16.1
2	26.3	92.1	31 August	2324	72	6.0	24.6	31 August	1437	34.0	23.8
3	25.7	96.8	1 September	2358	118	7.2	25.7	2 September	0622	32.0	22.4
4	24.4	95.9	2 September	0530	62	7.9	30.0	2 September	0622	41.6	29.1†

*r = Radial distance from WARF measured center to location of wave height measurement. †Average of wind speeds north and south of the aircraft.

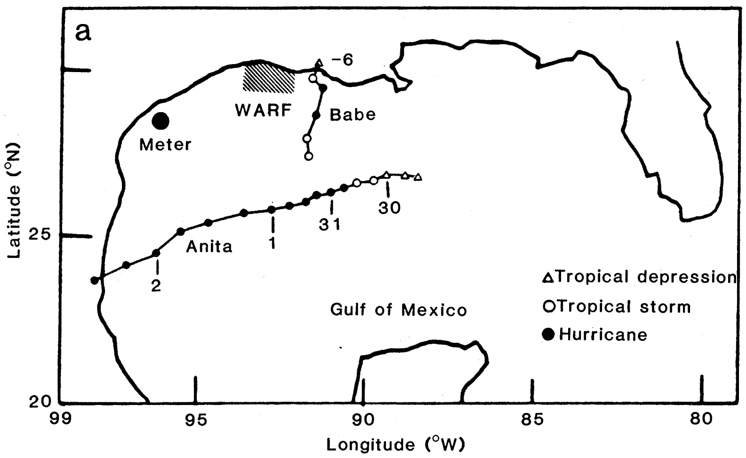

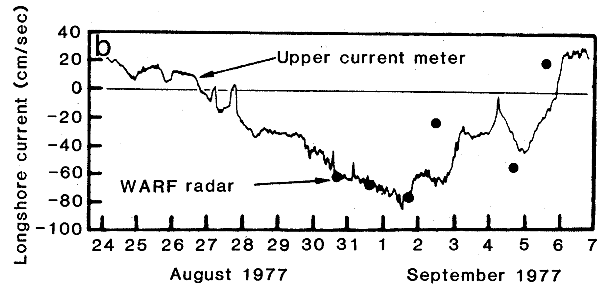

Fig. 10. Location (a) and results (b) of WARF radar and current-meter observations made during hurricanes Anita and Babe (30 August to 6 September 1977) (*41*). Continuous current record reproduced from figure 2 of Smith (*42*).

short-lived storm—developed. The tracks of Anita and Babe are also shown. We used the land echo appearing in the Doppler spectra to remove ionospheric motion effects from our data. Smith (*42*) measured the current speed and direction during this same period nearly 290 km to the west of the WARF measurements, at a location approximately 21.5 km off the Texas coast near Port O'Connor. Two recording current meters were deployed at 2 m and 10 m above the bottom in approximately 17 m of water. The time-averaged longshore component of current measured by Smith and reported at 1-hour intervals at this location is shown by the continuous curve in Fig. 10b. Positive values indicate motion toward 62°. The measurements of surface current made by the WARF radar are shown by dots in Fig. 10b.

Before Anita developed, the current-meter record showed currents of 10 to 20 cm/sec moving toward 62°. As the peripheral winds of Anita impacted the coastal regions, the currents reversed direction in response to the winds and steadily increased to a maximum value of approximately 80 cm/sec directed toward 242°. After the storm made landfall on 2 September, the magnitude of the current decreased until late on 4 September. At this time, another increase in the current magnitude was observed. Finally, the current reversed direction back to 62° on 6 September. The two current maxima found on 1 September and 5 September were caused by hurricanes Anita and Babe. The WARF radar estimates are in good agreement with the current meter observations. Again, direct quantitative comparison is not possible because of the large 290-km separation in distance between the two measurements. Anita tracked approximately parallel to the coastline. Because the radar beam was aligned to within 11° of the coastline, we assumed that the radar-measured component of the surface current was equivalent to the longshore current; this assumption is good to within 2 percent. The perpendicular distance between the two measurement points and the track are approximately equal, and we therefore observe, as expected, similar magnitudes but a different phase of the longshore current at each measurement point. The WARF radar estimates of the current precede those measured by the meter. In addition, the currents generated by Babe are greater at the location of the WARF radar measurements than at the location of the current meter.

Spatially averaged hurricane wind speed, wind direction, and wave height estimates made at the WARF for Anita were compared to point measurements made at NDBO buoys and by reconnaissance aircraft. Agreement was within the nominal measurement accuracy of all the sensors. Surface current measurements made by other sensors coincident with the radar measurements are rare. Comparison of point current measurements made nearly 290 km apart during Anita by the WARF radar and moored ocean current meters show reasonable agreement.

Conclusions

The WARF data set is not limited to the results presented in this article. Other analyses of the radar data that were not obtained in the vicinity of the buoy are also available. These experiments indicate that during a hurricane, HF skywave radar can provide ocean surface data that are as accurate as the more conventional measurements obtained in situ. The supportive surface data supplied by the WARF radar would prove particularly useful for tracking during early formative stages of hurricanes when multiple centers may be observed or when cirrus shielding may obscure visual location by satellite cloud photography. The high-resolution, large-coverage area, real-time steering, and continuous monitoring capabilities are unique to skywave radar. The hurricane data obtained from skywave radar complements data obtained from satellites, aircraft, and buoys.

References and Notes

1. Stanford Research Institute, "SRI remote measurements laboratory research capabilities" (Brochure, Stanford Research Institute, Menlo Park, Calif., 1977).
2. For further details on measurements of Anita and other hurricanes by HF skywave radar, see J. W. Maresca, Jr., and C. T. Carlson, "Tracking and monitoring hurricanes by HF skywave radar over the Gulf of Mexico" (Technical Report 1, contract F49620-76-C-0023, SRI International, Menlo Park, Calif., 1977); see also (*3*).
3. J. W. Maresca, Jr., and C. T. Carlson, *ibid.* (Final Report, contract F49620-76-C-0023, SRI International, Menlo Park, Calif., 1978).
4. D. D. Crombie, *Nature (London)* **175**, 681 (1955).
5. D. E. Barrick, *IEEE Trans. Antennas Propag.* **AP-20**, 2 (1972).
6. ——, in *Remote Sensing of the Troposphere*, V. E. Derr, Ed. (Government Printing Office, Washington, D.C., 1972), chap. 12.
7. T. M. Georges and J. W. Maresca, Jr., *Radio Sci.* **14**, 455 (1979).
8. J. R. Barnum *et al.*, *IEEE Trans. Antennas Propag.* **AP-25**, 128 (1977).
9. J. W. Maresca, Jr., and J. R. Barnum, *Mon. Weather Rev.* **107**, 1648 (1979).
10. M. S. Longuet-Higgins, D. E. Cartwright, N. D. Smith, in *Ocean Wave Spectra* (Prentice-Hall, Englewood Cliffs, N.J., 1963), pp. 111-136.
11. J. A. Ewing, *J. Mar. Res.* **27**, 163 (1969).
12. H. Mitsuyasu, F. Tasai, T. Syhara, S. Mizuno, M. Ohkusu, T. Honda, K. Rikiishi, *J. Phys. Oceanogr.* **5**, 750 (1975).
13. R. H. Stewart and J. R. Barnum, *Radio Sci.* **10**, 853 (1975).
14. D. E. Barrick, J. M. Headrick, R. W. Bogle, D. D. Crombie, *Proc. IEEE* **62**, 673 (1974).
15. D. E. Barrick, M. W. Evans, B. L. Weber, *Science* **198**, 138 (1977).
16. R. H. Stewart and J. W. Joy, *Deep-Sea Res.* **21**, 1039 (1974).
17. J. W. Maresca, Jr., R. R. Padden, R. T. Cheng, E. Seibel, *Limnol. Oceanogr.*, in press.
18. J. W. Maresca, Jr., J. R. Barnum, K. L. Ford, paper presented at the 1976 Annual Meeting of USNC/URSI, University of Massachusetts, Amherst, 11 to 15 October 1976.
19. J. W. Maresca, Jr., and K. L. Ford, "HF skywave radar measurement of the surface current in the North Pacific Ocean" (Technical Note RML-TN-9, Stanford Research Institute, Menlo Park, Calif., 1976).
20. D. E. Barrick, *Radio Sci.* **12**, 415 (1977).
21. J. W. Maresca, Jr., and T. M. Georges, *J. Geophys. Res.*, in press.
22. D. E. Barrick, *Remote Sensing Environ.* **6**, 201 (1977).
23. B. J. Lipa, *Radio Sci.* **12**, 425 (1977).
24. ——, *J. Geophys. Res.* **83**, 959 (1977).
25. D. E. Barrick and B. J. Lipa, in *Ocean Wave Climate*, M. D. Earle and A. Malahoff, Eds. (Plenum, New York, 1979), pp. 129-201.
26. B. J. Lipa and D. E. Barrick, *Radio Sci.*, in press.
27. ——, J. W. Maresca, Jr., in preparation.
28. J. W. Maresca, Jr., in *Ocean Wave Climate*, M. D. Earle and A. Malahoff, Eds. (Plenum, New York, 1979), pp. 221-234.
29. K. Hasselmann, D. B. Ross, P. Muller, W. Sell, *J. Phys. Oceanogr.* **6**, 200 (1976).
30. D. B. Ross, "A simplified model for forecasting hurricane generated waves," paper presented at Conference on Atmospheric and Oceanic Waves, American Meteorological Society, Seattle, Washington, 29 March to 2 April 1976.
31. V. J. Cardone and D. B. Ross, in *Ocean Wave Climate*, M. D. Earle and A. Malahoff, Eds. (Plenum, New York, 1979), pp. 61-91.
32. D. B. Ross and V. J. Cardone, in *Proceedings of NATO Symposium on Turbulent Fluxes Through the Sea Surfaces, Wave Dynamics and Prediction* (Plenum, New York, in press).
33. V. J. Cardone, D. B. Ross, M. R. Ahrens, in *Proceedings of the 11th Technical Conference on Hurricanes and Tropical Meteorology*, Miami, Florida, 13 to 16 December 1977.
34. J. W. Maresca, Jr., and C. T. Carlson, *J. Geophys. Res.*, in press.
35. ——, in *Proceedings of the 16th Conference on Coastal Engineering*, Hamburg, Germany, 27 August to 3 September 1978.
36. ——, in *Proceedings No. 263 Special Topics in Propagation (AGARDU)*, V. J. Coyne, Ed. (Technical Editing & Reproduction, London, 1979).
37. U.S. Army Coastal Engineering Reseach Center, *Shore Protection Manual* (Government Printing Office, Washington, D.C., 1973).
38. R. C. Sheets, *Mariner's Weather Log* **22** (No. 1), 1 (1978).
39. V. J. Cardone, "Specification of the wind distribution in the marine boundary layer for wave forecasting" (Report TR 69-1, Geophysical Science Laboratory, New York University NTIS, No. AD702490, 1969).
40. R. L. Elsberry, N. A. S. Pearson, L. B. Corgnati, Jr., *J. Geophys. Res.* **79**, 3033 (1974).
41. J. W. Maresca, Jr., and C. T. Carlson, *ibid.* **85**, 1640 (1980).
42. N. P. Smith, *ibid.* **83** (No. C12), 6047 (1978).

43. This work was supported by the Air Force Office of Scientific Research (AFOSR) under contract F9620-76-C-0023 and NOAA under contract 03-7-022-3511. We thank G. Glassmeyer, W. Preuss, G. Tomlin, and C. Powell of SRI for help in collecting data at WARF; D. Westover and W. Weir for writing the real-time sampling and post-processing software; and L. Laine, B. Richards, and J. King for typing the manuscript.
* This article is adapted from papers presented at the meeting of the Advisory Group for Aerospace Research and Development (AGARD), Lisbon, Portugal, 28 May to 1 June 1979, and the 16th Conference on Coastal Engineering, Hamburg, Germany, 27 August to 3 September 1978.